



<p>HORIZON 2020</p>   <p>Terahertz based Ultra High Bandwidth Wireless Access Networks</p>		Deliverable ID:	Preparation date:
		D3.4	11 April 2019
		Milestone: Final proposed	
		Title:	
		<p>Report on the design and simulation of THz integrated antennas</p>	
		Editor/Lead beneficiary (name/partner):	
		Luís Pessoa /INESC	
		Internally reviewed by (name/partner):	
		Thomas Kuerner (TUBS)	
		Cyril Renaud (UCL)	
		Approved by:	
		PSC / tbc	
Dissemination level			
PU	Public		
CO	Confidential, only for members of the consortium (including Commission Services)		X

Revisions				
Version	Date	Author	Organisation	Details
1.0	02/07/2018	Erick Lima	INESC	Initial Draft
1.1	18/09/2018	Luis Pessoa	INESC	Final version, ready for review
1.2	12/10/2018	Erick Lima	INESC	Revised according to reviewer's comments
1.3	21/03/2019	Luis Pessoa	INESC	Revised to address RP1 reviewer comments

Table of contents

Table of contents	2
List of Figures.....	3
Abbreviations	4
1 Introduction	6
1.1 Relationships with other deliverables	6
1.2 Structure of this document	6
1.3 Contributors	6
2 Overview of sub-THz antennas	7
2.1 Microstrip antennas	8
2.2 Coupling of microstrip antenna.....	10
2.3 Antenna efficiency	12
2.4 Antenna Directivity and Gain	13
2.5 Antenna bandwidth	13
3 Characterisation of microstrip antennas by simulation	14
3.1 Analysis of the radiation efficiency and directivity	15
3.2 Preliminary proposed design.....	17
4 Proposals for efficiency improvements	19
4.1 Conductor thickness evaluation	19
4.2 BCB and Polyimide Stack-up	22
5 Conclusion	25
6 Ongoing and Future work.....	26
References	27



List of Figures

Figure 1: Different possible shapes of microstrip antennas. [7].....	8
Figure 2: Illustration of a microstrip antenna. [7]	9
Figure 3: Different microstrip antenna feed typologies. [7].....	11
Figure 4: First order equivalent model for the different feed techniques. [7]	12
Figure 5: Gain and directivity flow chart. [9].....	12
Figure 6: Illustration of the microstrip antenna designed in HFSS considering the patch length equal to 290 μm and patch width equal to 300 μm	15
Figure 7: Fundamental parameters of the rectangular patch antenna as a function of substrate the thickness and patch width.....	16
Figure 8: Illustration of proposed microstrip antenna design considering a slot in order to provide a bandwidth enhancement.	17
Figure 9: Patch antenna current distribution at two different modes corresponding to 288 and 305 GHz.	17
Figure 10: Preliminary results of the proposed 15 μm BCB thickness rectangular slot patch antenna.	18
Figure 11: Radiation pattern of the presented antenna for 288, 295 and 305 GHz, respectively.....	18
Figure 12: Isometric and side view of 4 μm BCB/Polyimide and 4 μm conductor (gold) thickness.	20
Figure 13: Efficiency as a function of conductor thicknesses considering 4 μm BCB/Polyimide substrate	21
Figure 14: Radiation efficiency for both BCB and Polyimide considering different values of conductor thicknesses, {0, 1 and 4} μm , respectively.....	21
Figure 15: Peak radiation efficiency as a function of conductor thicknesses for both BCB and Polyimide considering zero tangent loss.....	22
Figure 16: Isometric and side view of the proposed multilayer design. Each BCB/Polyimide layer has 4 μm thickness separated with 0.1 μm thick of glass substrate. The ground plane and the antenna are both composed by 0.2 μm thicknesses of gold metal.	23
Figure 17: Radiation efficiency considering different layers of BCB/Polyimide without considering substrate loss.....	24
Figure 18: Radiation efficiency with and without considering substrate loss. The substrate loss causes almost 15 % reduction in efficiency.	24



Abbreviations

For convenience, provided below is a list of some of the abbreviations used in this document.

BCB	Benzocyclobutene
InP	Indium Phosphide
FB	Fractional Bandwidth
HFSS	High Frequency Structure Simulator
FEM	Finite Element Method
PEC	Perfect Electric Conductor
$\tan\delta$	Tangent loss
ϵ_r	Relative dielectric permittivity
σ	Electric conductivity
P_{rad}	Radiated power
P_{accep}	Accepted power
P_{diss}	Dissipated power
η	Radiation efficiency
S_{11}	Reflection coefficient
Z_{in}	Input impedance
$\text{Real}(Z_{in})$	Real part of the input impedance
$\text{Img}(Z_{in})$	Imaginary part of the input impedance



Executive summary

In this document, the feasibility of planar antennas using Benzocyclobutene and Polyimide substrates operating in the sub-THz range are investigated. In order to understand under which conditions the requirements of efficiency and bandwidth can be fulfilled, we evaluate the antenna performance as a function of substrate thickness and its physical dimension. In particular, we analyze how the BCB substrate thickness can affect the figures of merit of a patch antenna operating at 300 GHz such as efficiency, bandwidth, directivity and input impedance. From the presented analysis, we conclude that the antenna performance is governed by the substrate thickness, which has a strong impact on the radiation efficiency and impedance bandwidth. This means that the substrate thickness must be chosen according to the requirements of efficiency and bandwidth. We further conclude that the minimum acceptable thickness that can provide a peak efficiency up to 60% and fractional bandwidth (FB) up to 18% must be 15 μm . These conclusions should be taken into account in the subsequent antenna fabrication work.



1 Introduction

1.1 Relationships with other deliverables

The antenna designs presented in this document relate to the following deliverables:

- D3.6 Second generation of devices for integration and packaging. This deliverable will present integrated designs for phased array antenna integration. Reporting on the phase distribution design and substrate antenna manufacturing will also be included.
- D3.7 Final delivery of devices for integration and packaging. This deliverable will present the transmitter design at 300 GHz with improved efficiency. The transmitter chip design for integration with the phase distribution PIC and substrate antenna will be included. The deliverable will include a report on the integrated antenna and phase distribution PIC characterization ready for integration.
- D3.8 Final packaged devices. This deliverable will present the final devices with integrated multiple modules and components which will be packaged for full delivery in WP4 and WP6 for the final demonstration.

1.2 Structure of this document

This document is structured in three main sections: Section 2 presents a brief review of the sub-THz antenna technology relevant for this project as well as a review of microstrip antennas. Section 3 presents the performance analysis of a rectangular patch antenna operating at 300 GHz as a function of substrate thickness, including a preliminary proposed design of a 15 μm BCB thickness patch antenna. Lastly, in section 4 we discuss alternative techniques for improving the antenna performance.

1.3 Contributors

The following partners have contributed to this deliverable:

- INESC (Erick Lima, Luís Pessoa)
- UGLA (Edward Wasige, Abdullah al Khalidi)
- UCL (Cyril Renaud, James Seddon)



2 Overview of sub-THz antennas

Sub-Terahertz wireless communications require power sources and antennas properly designed to meet special requirements, such as bandwidth, efficiency and output power. In addition to these, good power coupling efficiency between sources and antennas is desired in order to maximize the radiated power, and consequently the efficiency of the overall system.

The need for good power coupling efficiency and radiation efficiency is motivated by the low power levels achieved by the sources, which is one of the major challenges in THz technology. So far, the achieved output power is in order 1 mW at 300 GHz for RTDs and UTC-PDs. Furthermore, small and compact devices are desired to achieve space miniaturization and cost reduction, which requires antenna integration. Therefore, THz RTDs and UTC-PD sources, integrated with antennas, are still at a research level, although some prototypes have been successfully demonstrated [1]–[3].

In the first generations of these systems, the antennas were typically designed in the devices host semiconductor, typically Gallium Arsenide (GaAs) or Indium Phosphide (InP). However, such semiconductors have a high dielectric permittivity ($\epsilon_r \approx 12$), which makes the control of the radiation pattern and input impedance a difficult task. To alleviate these problems, lens antennas were proposed. However, this approach leads to a poorly efficient and larger device [4]–[6].

Recently, new approaches have been proposed, which consist of stacked layers of different substrates. In this approach, the active part is created in the high permittivity semiconductor, which is separated from the antenna substrate by a metal layer. The antenna layer typically consists of BCB or Polyimide with dielectric constants of 2.6 and 3.5, respectively. In this way, upward radiation can be achieved without much effort and the total dimension of the source integrated with the antenna can be reduced. An antenna on a 7 μm -thick BCB substrate operating at 510 GHz was presented in [1], [2], integrated with a resonant-tunneling-diodes (RTD). Additionally, simulation results of a 50 μm BCB thickness bow-tie antenna operating at 300 GHz was presented in [6]. The authors of these works concluded that improvements in the overall results can be achieved by considering a better power coupling efficiency between the sources and the antennas. To achieve that, the antennas input impedance and the sources output impedance must be considered at the design stage, so a proper matching can be performed.

Considering BCB or Polyimide technology as antenna substrates, separated from the high dielectric constant semiconductor by a metal layer, implies one of the two configurations: using the metal layer as a reflector plane or as a ground plane. In order to use the metal layer as a reflector plane, the antenna must be positioned at a certain fraction of the wavelength distant from the reflector. The optimal distance is usually fixed around $\lambda/4$ ($\approx 150 \mu\text{m}$ at 300 GHz for $\epsilon_r = 2.6$), which is much longer than the requirement of 3 – 4 μm thickness established by consortium partners (UGLA and UCL). Thus, we conclude that the most appropriate configuration to be integrated with the oscillators are microstrip antennas, also known as patch antennas. In a microstrip antenna, the metal layer acts as a ground plane instead of a reflector plane and the thickness can be significantly decreased compared to the case of using it as a reflector.



2.1 Microstrip antennas

Microstrip antennas date back to the 1970's and they have been used in several applications due to their simplicity and versatility. Microstrip antennas are easy to design and fabricate, allow for compact solutions since they can be integrated in a single printed circuit board (PCB) with active components allowing single board wireless transceivers, and present features that can fulfill the requirements of many applications despite their narrowband capability and low efficiency. Recently, microstrip antennas have been applied in the THz frequency range combined with state-of-the-art THz sources such as RTDs and UTC-PDs. In these emerging technologies, microstrip antennas offer the interesting features of being compact and at the same time allowing the antenna to be designed in low dielectric permittivity ($\epsilon_r \leq 3$) substrates, which is isolated from high dielectric permittivity ($\epsilon_r \geq 10$) substrates by means of a ground plane. This approach allows the canceling of substrate wave modes and makes upward radiation feasible. Many configurations have been proposed to enhance microstrip antenna bandwidth, such as, stacked parasitic layers, employment of coplanar parasitic elements and slot configurations, achieving fractional bandwidths (FW) of about 30 % [7]–[12], when normal values reside between 5-7 %. These techniques consist in achieving multiple resonance frequencies, which when properly combined allow for impedance bandwidth enhancements. Although a single resonant element could be used with an additional matching network to extend the bandwidth, the multi-resonance techniques are predominantly preferred. The most direct method for efficiency improvement consists in increasing the substrate thickness, leading to 60-80 % efficiency. Although in most practical cases it is not reasonable to ignore substrate loss and surface waves. If we could neglect them, efficiencies up to 90 % would be possible simply by increasing the substrate thickness.

A simple microstrip antenna is composed of a thin layer metal patch, which constitutes the radiating element, a substrate material or combinations of different substrate layers, a ground plane and the feeding line. Even though the radiating element can take any of the design forms illustrated in Figure 1 [13] or even others not shown in the list, being only limited by the designer imagination and needs, the square, rectangular and circular ones are preferred in most of the time due to their simplicity.

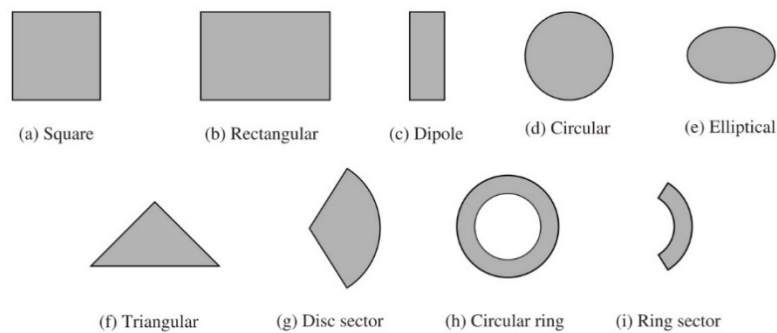


Figure 1: Different possible shapes of microstrip antennas. [7]

Figure 2, illustrates a square patch fed by a microstrip line. Its resonance frequency is mainly determined by the physical length of the radiating element, L , which is calculated as a function of the substrate properties, ϵ_r, h , the relative electric permittivity and thickness, respectively, to satisfy the equation $L = \frac{\lambda}{2} + \Delta l$, where λ is the wavelength given by $\frac{1}{f\sqrt{\mu_0\mu_r\epsilon_0\epsilon_r}}$, in which ϵ_0 and μ_0 are free space electric permittivity and magnetic permeability, respectively. The Δl factor is used to compensate the fringing fields effect and, although theoretically quantified, in terms of design it is often obtained by means of parametric simulations or optimizations algorithms. The width of the patch, W , does not have a significant impact on the resonance frequency, but it allows for improvements on the bandwidth and



efficiency since its increase leads to a conduction loss reduction. However, these improvements resulting from increasing the patch width are valid only up to a certain point, where undesirable current distributions start to take place, which can cause unwanted radiation pattern effects.

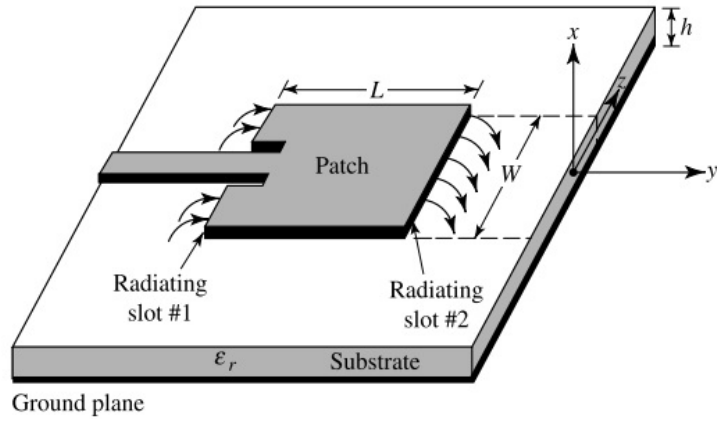


Figure 2: Illustration of a microstrip antenna. [7]

The microstrip antenna can exhibit different radiation patterns depending on the current distribution that has been excited on it. Despite the complexity involved in the theoretical study, the current distribution analysis can be performed by means of the cavity model, using an Eigenmode solver or even considering a full wave simulation, for a better understanding of what current modes can fulfill design requirements or for getting some insight into the working principle of the structure. The resonance frequency of the first mode (TM_{010}), which is the one desired in almost all practical cases can be calculated by means of the following equation [13]:

$$(f_r)_{010} = \frac{1}{2L\sqrt{\epsilon_r}\sqrt{\mu_0\epsilon_0}} = \frac{v_0}{2L\sqrt{\epsilon_r}} \quad (1)$$

where v_0 corresponds to the speed of light in free space. The current density distribution, $\vec{J}_s = \hat{n} \times \vec{H}$, of the TM_{010} mode is maximum at the center of the radiating element and minimum at the ends, and from the cavity model, the electric and magnetic field on the radiating element can be approximately expressed as [14],

$$\text{vertical electrical field} = E_x = E_0 \cos \frac{\pi y}{L}, \quad (2)$$

$$\text{transverse magnetic field} = H_z = H_0 \sin \frac{\pi y}{L}. \quad (3)$$

Note that equations (2) and (3) are referred to the coordinated system shifted to the left edge of the antenna (towards the feeding point). For example, the electric field is maximum at the edge, where $y = 0$, minimum at the center of the path, where $y = L/2$, and maximum once again at the right edge, corresponding to $y = L$. The magnetic field is referenced in the same coordinates being 90° out of phase of the electric field. Also, this equation reveals that this quantity remains constant in the z – axis.

The TM_{010} mode leads to a radiation pattern with a maximum in the normal plane to the antenna (xy – plane) in the upward direction and a minimum at the edges. For example, an observer in the elevation plane (xy – plane, positive side) aligned with the center of the radiating element should receive a maximum while an observer in the azimuth plane (zy – plane) aligned with the (y – axis) should receive a minimum.



The patch antenna can also be modeled as an open-ended transmission line, in which the voltage and current can be approximated as,

$$\text{voltage} = V(y) = V_0 \cos \frac{\pi y}{L}, \quad (4)$$

$$\text{current} = I(y) = \frac{V_0}{Z_0} \sin \frac{\pi y}{L}, \quad (5)$$

and, since $Z_{in} = \frac{V(y)}{I(y)}$, this means that the impedance varies through the length of the patch, remaining constant across its width. Once again, this equation is referred to the coordinated system shifted to the left edge of the antenna (towards the feeding point). For example, the impedance is maximum at the edges, achieving values of hundred ohms and a minimum at the center. The optimal feed point, considering a 50-ohm power source matched to a 50-ohm transmission line, is often found around $y = \frac{L}{4}$ from the edge. This is the reason why in **Figure 2**, the microstrip line goes into the patch for better impedance matching.

2.2 Coupling of microstrip antenna

A microstrip antenna can be fed considering various topologies, to name: microstrip feed, aperture feed, magnetic coupling and capacitive coupling. Illustrations of the different mechanisms are presented in Figure 3 [13]. Among them, the microstrip feed is the simplest one, consisting of a microstrip line that feeds the antenna as illustrated in Figure 3 (a). The input impedance of the TM_{010} mode can be controlled by adjusting the position of the feed line into the antenna, which is commonly known as inset feed. As we introduced before, this technique takes advantages of the fact that the impedance varies across the length of the patch, so by moving the feed point into the antenna it is possible to find an optimum position for a certain desired input impedance. However, as the substrate thickness increases the microstrip line starts to produce spurious radiation which can affect the radiation pattern and the antenna efficiency. Besides that, this feeding technique is not so convenient in cases when the power source and the antenna do not share the same plane.

Another well known feeding technique is the coaxial feed, illustrated in Figure 3 (b). In this case the outer shielding of the transition line is connected to the ground plane and the inner side is connected on the patch. This feeding technique suffers from parasitic inductance limitations that result from the feed line length being proportional to the substrate thickness, and therefore it is not recommended for antenna arrays. Similarly, to the microstrip feed, the input impedance can be controlled adjusting the feed position.

In order to overcome the limitations presented by microstrip and coaxial feed options, aperture-coupled feed and proximity coupled feed approaches were proposed. The aperture feed, Figure 3 (c), consists in having two different substrates separated by a metal layer. The feeding line is then designed in the bottom part of the first substrate layer and the antenna is designed on the top of the second one. The feeding is reached by means of an aperture in the middle metal layer which is the shared ground plane by the patch and the microstrip feed line. The aperture can take many shapes, however, the rectangular one is the most common. The input impedance can be controlled adjusting the length of the feed line, the position and size of the slot. The proximity feed, also known as magnetic coupling feed, often consists of two substrate layers as illustrated in Figure 3 (d). The feeding line consists of a microstrip line between the two layers which induces a current distribution on the patch. The input impedance is mainly controlled by adjusting the length of the transmission line and the ratio between patch and feed line widths.

Figure 4 presents equivalent models for the different feeding methods. As it is possible to observe, the microstrip and coaxial feed approaches present similar equivalent models, exhibiting an inductive behavior. The proximity feed exhibits a capacitive behavior and the aperture feed present both capacitive and inductive coupling mechanisms. It is important to note that all the equivalent models



correspond to the fundamental mode TM_{010} . In case of more than one mode, for example, if a parasitic element is employed for bandwidth enhancement, these equivalent models are no longer valid, and more complex models must be derived in case the modelling of the antenna in terms of lumped component is required.

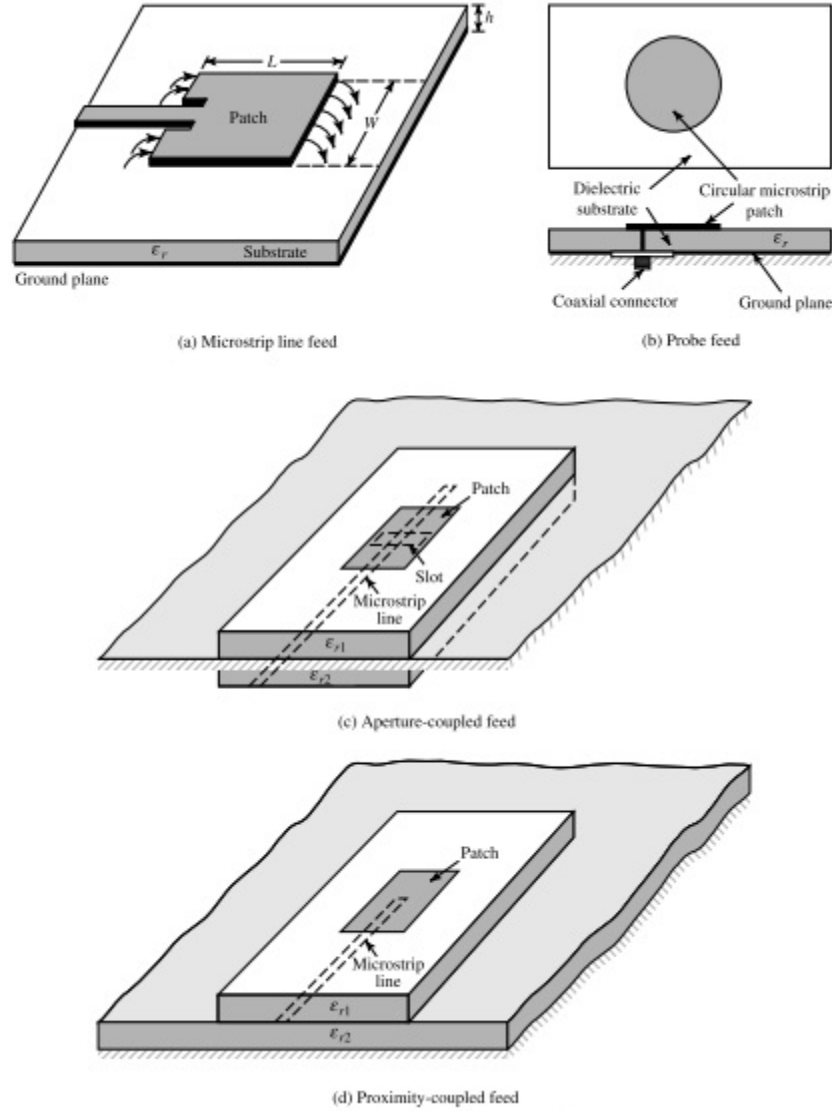


Figure 3: Different microstrip antenna feed typologies. [7]



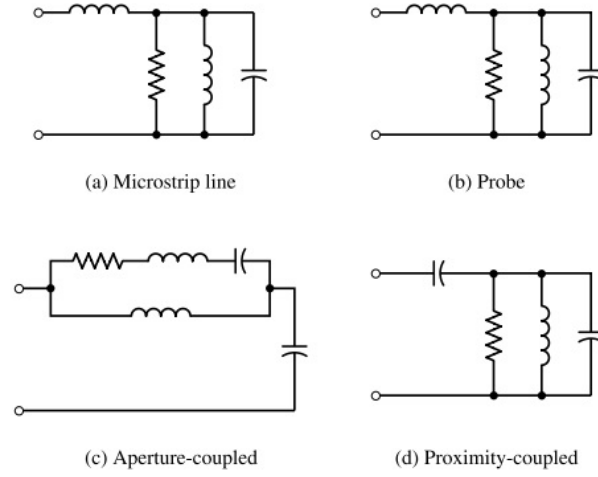
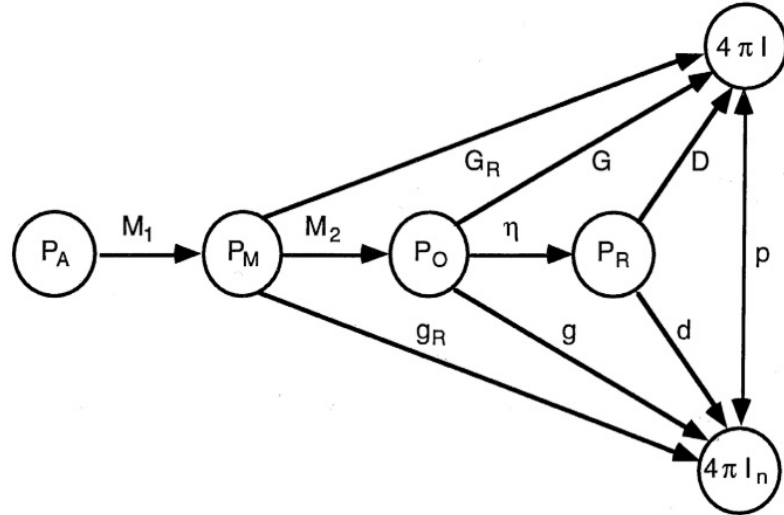


Figure 4: First order equivalent model for the different feed techniques. [7]

2.3 Antenna efficiency



P_A = power available from the generator
 P_M = power to matched transmission line
 P_O = power accepted by the antenna
 P_R = power radiated by the antenna
 I = radiation intensity
 I_n = partial radiation intensity[†]
 M_1 = impedance mismatch factor 1
 M_2 = impedance mismatch factor 2

η = radiation efficiency
 G_R = realized gain
 G = gain
 D = directivity
 g_R = partial realized gain
 g = partial gain
 d = partial directivity
 p = polarization efficiency

Figure 5: Gain and directivity flow chart. [9]

Figure 5 [15], presents an intuitive view of some of the most important antenna parameters extracted from the IEEE standard definition of terms for antennas, in which efficiency is included, and the same original source also provides definitions for all the illustrated parameters. Antenna efficiency takes an important role in a wireless system, especially when small source powers are available (< 1 mW) and when the operation frequency is very high, which is the case of the sub-THz sources available in Terapod. The antenna efficiency depends on several factors including, substrate loss, conduction loss,



and surface waves since these do not contribute to the useful radiated power, P_R . The efficiency can be described mathematically as,

$$\eta = \frac{P_R}{P_R + P_{Loss}}, \quad (6)$$

where $P_o = P_R + P_{Loss}$, in which P_{Loss} is the fraction of the accepted power which is not radiated.

2.4 Antenna Directivity and Gain

According to the already mentioned IEEE standard, directivity is the radiation power intensity in a certain direction divided by the average radiated power by the same antenna. In mathematical form, it can be expressed as [13],

$$D = \frac{4\pi U}{P_{rad}}, \quad (7)$$

where P_{rad} denotes total radiated power and U denotes power intensity in a certain direction. The directivity of a microstrip antenna considering a single element resides mainly between 5 – 7 dBi. In most of the cases, the directivity bandwidth is greater than the impedance bandwidth, so the antenna bandwidth is mostly defined by the impedance bandwidth as we will show during this report.

The gain of an antenna “is the radiation power intensity in a certain direction over the total power that would be radiated by an isotropic (ideal) antenna receiving the same amount of power”. Therefore, the difference between directivity and gain is the efficiency, and then the gain (G_{max}) in a certain direction is expressed as:

$$G = \eta \frac{4\pi U}{P_{rad}}. \quad (8)$$

2.5 Antenna bandwidth

Antenna bandwidth is defined as “the range of frequencies within which the performance of the antenna, with respect to some characteristic, conforms to a specified standard.” The concept of antenna bandwidth extends beyond the impedance bandwidth since the directivity and efficiency must be considered. For example, an antenna is wideband if it has wideband impedance and both directivity and efficiency fulfil the requirements in the entire impedance bandwidth. The figure of merit that considers all these parameters is known as realized gain (RG). The realized gain in a certain direction takes into account the power reflected by the antenna towards the generator, conduction loss, substrate loss, surface waves radiation and radiated power.

In a microstrip antenna, the realized gain is dominated by the efficiency and the impedance bandwidth, since the directivity remains almost constant in a broad frequency range compared to the impedance bandwidth or efficiency. Usually, a microstrip antenna in its simple form has a fractional bandwidth (FB) of 5 %. Higher bandwidth can be achieved considering thicker substrates, employing parasitic elements or slot configurations. The bandwidth resultant from thick substrates is derived from the natural dependence of the Q – factor with the substrate height, while parasitic elements and slot configurations allow the excitation of more than one current mode, which results in multiple resonance frequencies, increasing the overall bandwidth.



3 Characterisation of microstrip antennas by simulation

In this section, we evaluate the performance of a rectangular microstrip antenna operating at 300 GHz as a function of the substrate height and antenna size. The study was carried out in the electromagnetic simulator software HFSS using the Finite Element Method (FEM). We used the default HFSS Benzocyclobutene (BCB) substrate with a relative permittivity of $\epsilon_r = 2.6$ and a hypothetically zero dielectric loss tangent, $\tan\delta = 0$, which allows us to take in to account only the radiation phenomena and ohmic losses in this first approach.

Since we observed that the substrate height governs the radiation efficiency of the patch antenna, it is important to characterize and understand how it can affect the performance of the antenna. Additionally, we found evidence that the efficiency is affected by the patch width, and so simulation results for different widths are presented as well. However, improvements in efficiency as a function of the patch width are achieved at the cost of an increase in the total area. Also, it is important to note that the patch width must be smaller than the ground plane by a certain fraction of the wavelength in order to decrease the backward radiation. In addition to the degradation of the radiation efficiency, bandwidth reduction is expected with the decrease in the substrate thickness (although not shown) as a direct consequence of the increase in the quality factor.

For a better understanding of what causes the efficiency degradation, we also calculated the conduction loss as a function of the substrate thickness and compared with the accepted and radiated power by the antenna. Both the efficiency obtained directly from HFSS and the one resulting from the quotient of the radiated power (P_{rad}) by the dissipated power (P_{diss}) showed good agreement, which validates the calculation of the conduction loss.

Contrarily to the radiation efficiency, we verified that the directivity is not significantly affected by the substrate thickness, as will be shown. Thus, the major impact is noted in the efficiency and impedance bandwidth.

Considering that the radiation efficiency and the directivity do not depend on the input impedance, we performed the study of those parameters while neglecting the impact on input impedance. At the end of this section, it will be clear that the antenna design is strongly governed by the thickness of the substrate. Therefore, it will be possible to start the design considering a substrate thickness that can provide an acceptable radiation efficiency and then start to optimize the realized gain and the impedance bandwidth.



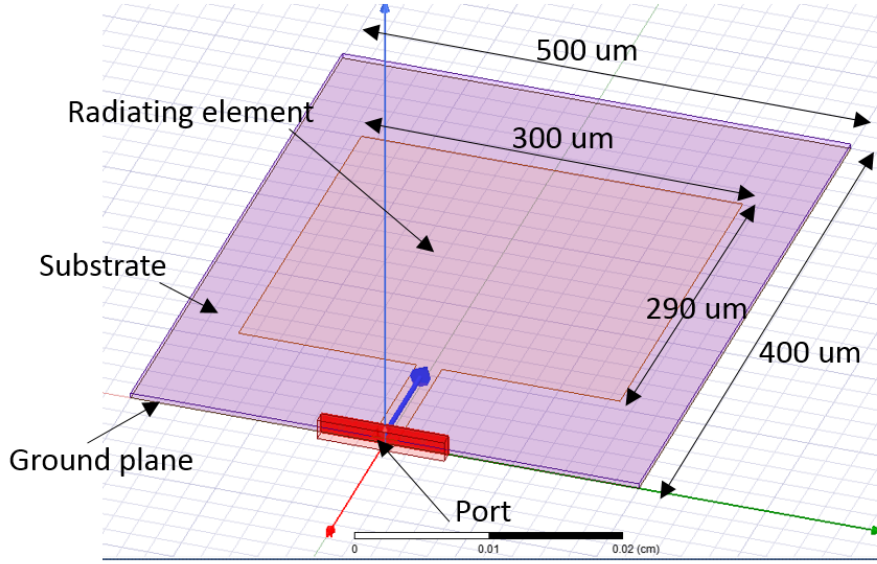


Figure 6: Illustration of the microstrip antenna designed in HFSS considering the patch length equal to 290 μm and patch width equal to 300 μm .

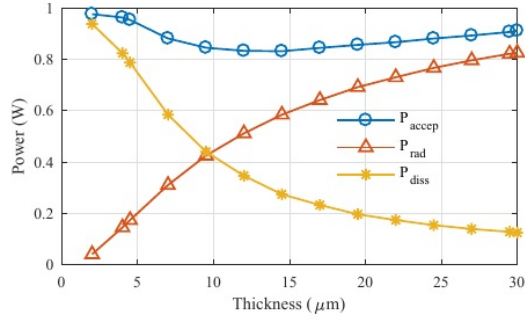
3.1 Analysis of the radiation efficiency and directivity

In order to evaluate the impact of the substrate thickness on the radiation efficiency, we fixed the length and width of the antenna at 290 and 300 μm (Figure 6), respectively. The BCB substrate has an area of $400 \times 500 \mu\text{m}^2$ and therefore the ground plane, which corresponds to a zero-thickness sheet of gold having an electric conductivity of $\sigma = 41 \times 10^6 \text{ S/m}$ has the same area. Analogous to the ground plane, the patch is modeled as a zero thickness gold sheet. Therefore, surface roughness and conductor thickness are not considered in this first approach. It is important to remember that the substrate does not affect the efficiency since we are also considering $\tan\delta = 0$.

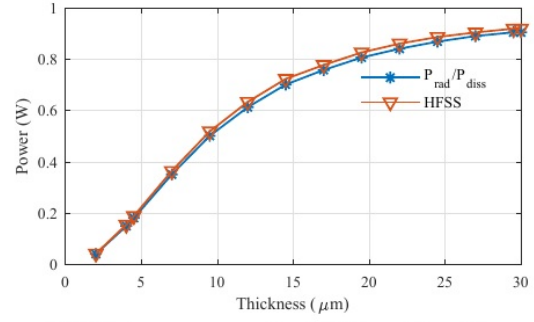
The layout of the antenna used in this section is illustrated in Figure 6. As it is possible to observe, we are using the microstrip feeding technique, which seems to us the most appropriate approach for this application, as already mentioned in section 2.2. In this preliminary analysis, we considered a simulation setup consisting of a wave port directly attached to the microstrip line, while in the next iteration of this work, the antenna will be coupled to a CPW line in order to facilitate the integration with the power source. Thus a CPW to microstrip line transition will be considered employing a technique similar to the one used by the authors of [16].

Figure 7 (a) depicts the antenna peak values for accepted power, represented by the "o" marker; dissipated power, represented by the "*" marker and radiated power, represented by the "Δ" marker. These parameters were evaluated for a substrate thickness (h in Figure 2) varying from 2-30 μm . By analyzing the figure, it is possible to observe that the accepted power (P_{accep}) remains above 0.8 W (with a source power of 1 W) within the entire considered thickness range.

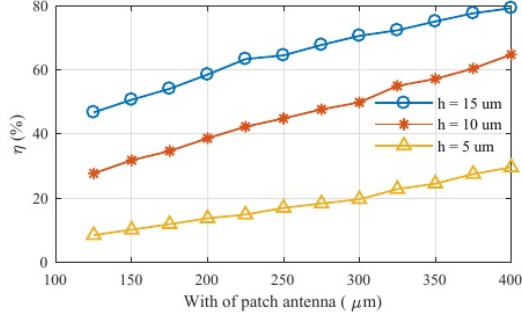




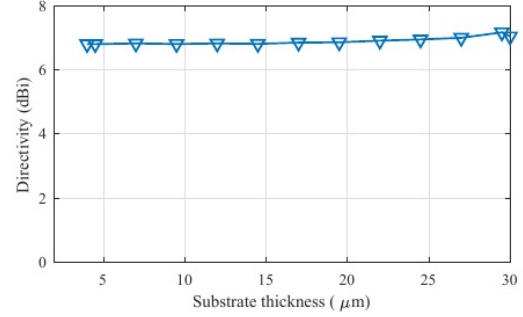
(a) Accepted power (P_{accept}), radiated power (P_{rad}) and dissipated power (P_{diss}).



(b) Efficiency reported by HFSS and $P_{\text{rad}}/P_{\text{diss}}$.



(c) Efficiency considering thickness = 5, 10, 15 μm .



(d) Directivity at the elevation plane for $\theta = 0$.

Figure 7: Fundamental parameters of the rectangular patch antenna as a function of substrate the thickness and patch width.

The accepted power can be improved by optimizing the antenna input impedance for each height. Although the accepted power is considerably high, even without optimization of the input impedance, the fraction of this power that is radiated is strongly governed by the substrate thickness. As it is possible to observe, the radiated power at 4 μm thickness is less than 40%, being all the rest dissipated in the conductor, while for thicknesses up to 15 μm , a fraction up to 60% of the accepted power is radiated.

Figure 7 (b) presents the radiation efficiency considering both the efficiency reported by HFSS and the efficiency obtained by $P_{\text{rad}}/P_{\text{diss}}$, showing a good agreement. As it is possible to observe, the efficiency curve exhibits a linear behavior up to 14 μm . After that, the efficiency grows slower, approximating to a theoretical maximum close to 100%.

We also evaluated the efficiency as a function of the antenna width considering three different thickness values of {5, 10, 15} μm as illustrated in Figure 7 (c). From that simulation, we concluded that the efficiency can also be increased by increasing the width of the antenna. Thus, it seems reasonable to conclude that the width of the antenna must be as large as possible since the fundamental microstrip mode is still present.

Figure 7 (d) shows that the directivity is almost independent of the substrate thickness as we mentioned before. Varying the thickness between 2 – 30 μm the curve does not exhibit any significant variation.



3.2 Preliminary proposed design

From the conclusions of the previous sections, we decided to select a 15 μm substrate height, which seems to us a minimum acceptable value to achieve a reasonable efficiency ($\geq 50\%$).

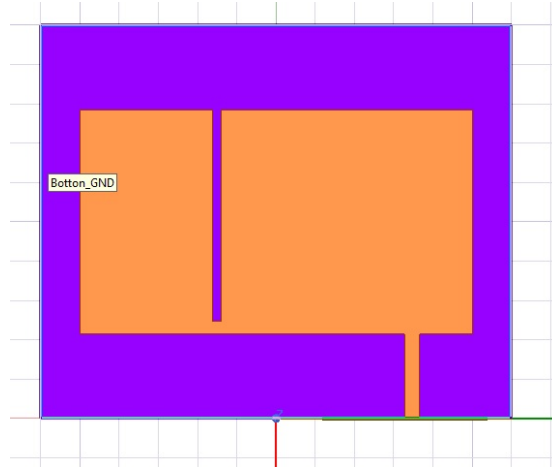


Figure 8: Illustration of proposed microstrip antenna design considering a slot in order to provide a bandwidth enhancement.

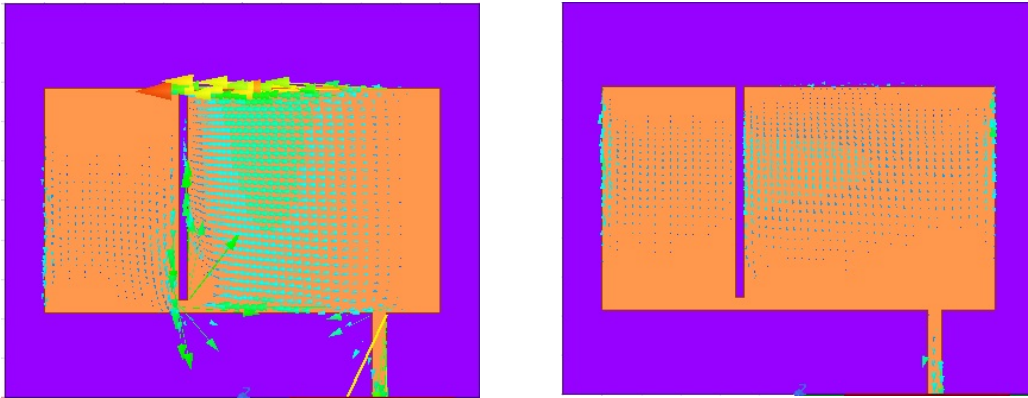


Figure 9: Patch antenna current distribution at two different modes corresponding to 288 and 305 GHz.

The patch length was initially calculated and optimized through simulation to resonate at 300 GHz. In order to increase the impedance bandwidth, we considered a slot (shown in Figure 8), which allows the excitation of two orthogonal current modes as illustrated in Figure 9. The feed and the slot position were optimized to allow the current modes to resonate at two distinct frequencies corresponding to 288 GHz and 305 GHz, respectively, as it is possible to observe from the magnitude of the S_{11} parameter as shown in Figure 10 (a). In this way, we achieved a bandwidth of 26 GHz, that corresponds to a $FB \approx$



18%. In the presented results, the feed line was de-embedded in order to consider only the antenna input impedance.

The directivity in the elevation plane, for $\theta = 0^\circ$ is up to 6.5 dBi in the overall frequency band as illustrated in Figure 10 (d). As is it possible to conclude from the figure, the directivity is not significantly affected by the substrate height, so the main focus should be placed in the radiation efficiency and impedance bandwidth. Figure 11 illustrates 3D radiation patterns for 288, 295, and 305 GHz showing the stability of the patterns across the impedance bandwidth.

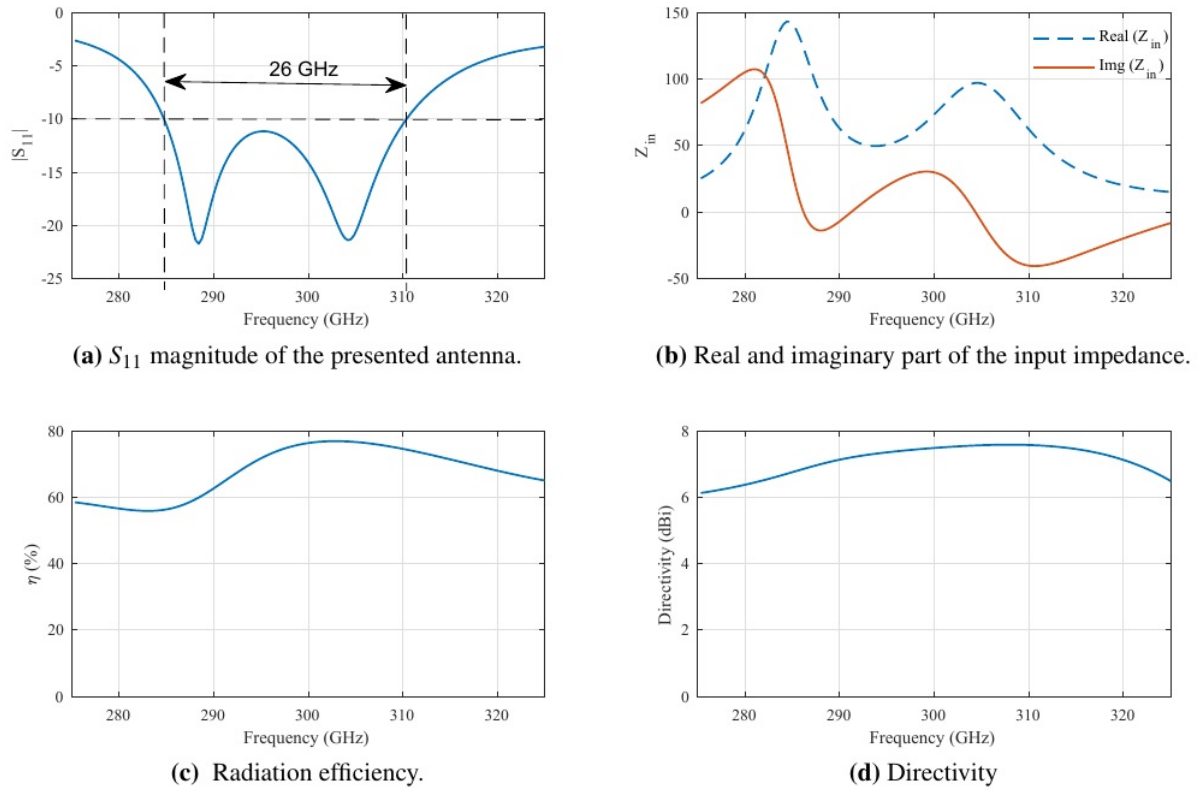


Figure 10: Preliminary results of the proposed 15 μm BCB thickness rectangular slot patch antenna.

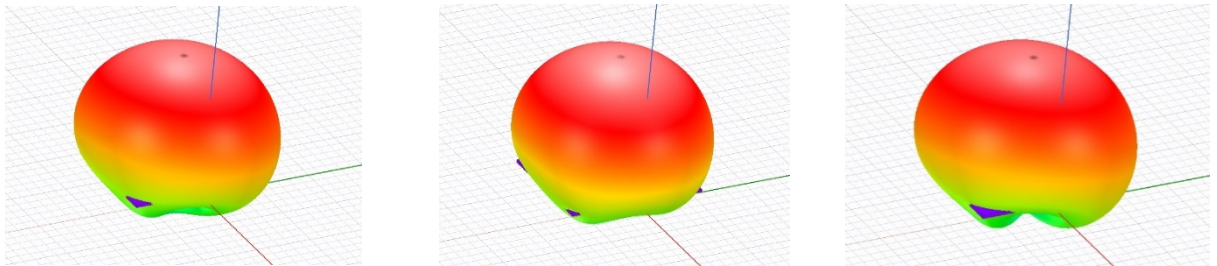


Figure 11: Radiation pattern of the presented antenna for 288, 295 and 305 GHz, respectively.



4 Proposals for efficiency improvements

As shown in the previous section, the radiation efficiency is mainly dominated by the substrate thickness. Through simulation results, we demonstrated that substrate thicknesses thinner than 15 μm lead to a poor radiation efficiency. For example, at 4 μm substrate thickness, which corresponds to the maximum value established from the requirements, the efficiency is not more than 20 % when an ideal zero-thickness conductor is considered. Although so far we have been considering the worst case of having a zero-thickness conductor, we will show in this section that even considering a feasible thickness conductor, the efficiency remains very poor ($< 30\%$) if a 4 μm thickness substrate is considered. We have been working toward solutions to overcome these limitations after we observed this limitation.

So far, we have proposed a 15 μm substrate thickness for the antenna design, which can potentially provide peak efficiencies up to 70%. In this section, we analysed and evaluated the performance of two design approaches. The first one consists in the use of a thick metal conductor. This approach requires conductor thicknesses up to 4 μm if an efficiency above 30 % is desired when considering a 4 μm substrate thickness. The second approach consists of a multilayer substrate design. We verified that a peak efficiency up to 70 % is achieved considering a substrate with 4 layers of 4 μm thickness (please see Figure 16). We separated the different layers with a very thin layer (0.1 μm) of glass substrate having $\epsilon_r \approx 5.5$. The use of glass is just to illustrate the concept; in fact, another material could be used. In fact, during an internal WP3 meeting between INESC and UGLA (at 09/08/2018) we concluded that an intermediate layer is not even necessary.

So far, in all the presented results, we have been considering only BCB substrate, nonetheless, the fundamental concepts and the limitations are almost the same for both BCB and Polyimide. In the subsequent results, we are going to consider both BCB and Polyimide substrates. We considered $\epsilon_r \approx 3.5$ for polyimide and $\tan_D = \{0, 0.008\}$ for different situations. The tangent loss (\tan_D) of 0.008 is the default value considered for Polyimide in HFSS and a reduction of at least 15% efficiency must be expected if it is considered.

4.1 Conductor thickness evaluation

The increase in the conductor losses that occur when the substrate becomes thinner is explained by the skin depth phenomena, which in turn depends on the conductor thickness. So far, we have been considered ideal zero thickness conductor (Perfect Electric Conductor - PEC), however, there is an optimal conductor thickness at which the conductor loss becomes minimum [17]. Therefore, a possible solution to decrease the substrate thickness maintaining a good efficiency is to increase the conductor thickness, an approach we explore below.

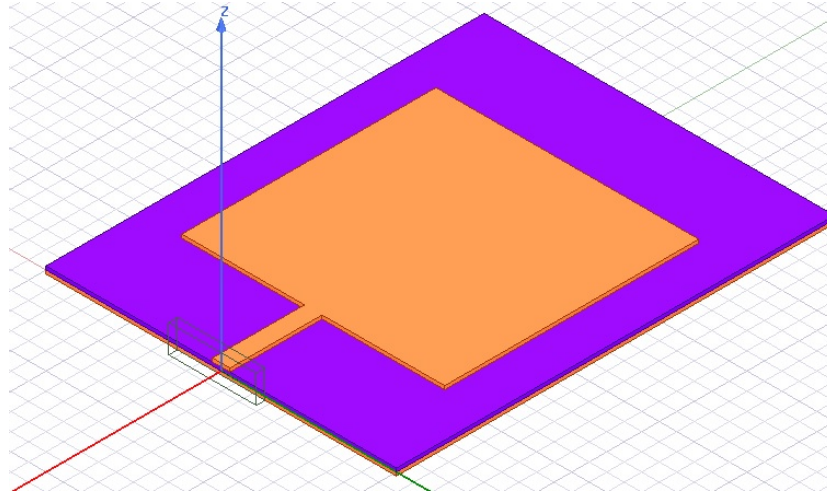
The current conductor thickness used in the devices fabricated within the context of this project is 0.2 μm , which allow us to reduce the substrate thickness from 15 μm to 10 μm with efficiency up to 48%. Considering a hypothetical conductor thickness of 4 μm allows us to achieve an efficiency up to 38 % at 6 μm substrate thickness. In order to reduce the substrate thickness down to 4 μm , while maintaining the efficiency above 20 %, a conductor thickness above 10 μm would be expected, which seems unfeasible.

Figure 12 shows a side view and an isometric view of the proposed microstrip antenna considering 4 μm conductor thickness and also 4 μm substrate thickness. Simulation results of the radiation efficiency considering conductor thicknesses varying from 0 to 10 μm (maintaining substrate thickness at 4 μm) with incremental steps of 0.2 μm (without considering substrate losses) is presented in Figure 13. From that figure it is possible to observe improvements in the peak radiation efficiency that vary from 10 % to 70 % corresponding to 0 and 10 μm conductor thickness, respectively. Additionally, Figure 14 depicts the radiation efficiency against frequency considering conductor thickness of $\{0, 1 \text{ and } 4\}$ μm . From this figure, it is possible to observe again the benefit of increasing the conductor thickness on the radiation efficiency. With 0 μm conductor thickness, the observed peak efficiency is only 10 %, which is improved up to 30 % when a conductor thickness of 1 μm is considered, while peak efficiency of 50 % is achieved considering a 4 μm thickness conductor. Additionally, it is possible to observe that

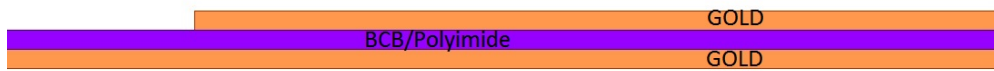


both BCB and Polyimide present similar performance if substrate loss is neglected. However, in order to obtain the same resonance frequency, the physical length of the antenna in polyimide is expected to be smaller than the one in BCB $\left(L = \frac{1}{2f_r\sqrt{\epsilon_r}\sqrt{\mu_0\epsilon_0}}\right)$ due to its higher permittivity.

Figure 15 illustrates the situation of considering Polyimide with 0 and 0.008 tangent loss. This figure shows the significant effect that the substrate loss causes on the radiation efficiency leading to a decrease around 30 %. In this situation, even considering a thick conductor, the peak radiation efficiency remains very poor. As it is possible to observe, the peak radiation efficiency remains at only 20 % even considering a conductor having 10 μm thickness. These observations lead us to conclude that to improve efficiency at the cost of increasing the conductor thickness seems to be unfeasible in our case.



a) Isometric view



b) Side view

Figure 12: Isometric and side view of 4 μm BCB/Polyimide and 4 μm conductor (gold) thickness.



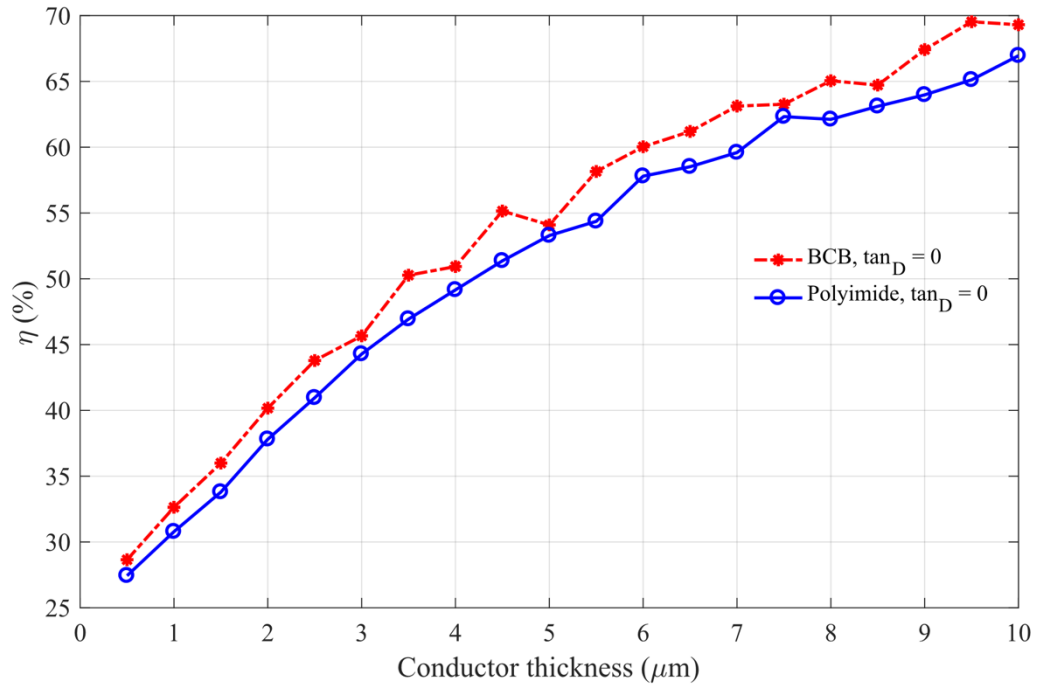


Figure 13: Efficiency as a function of conductor thicknesses considering 4 μm BCB/Polyimide substrate

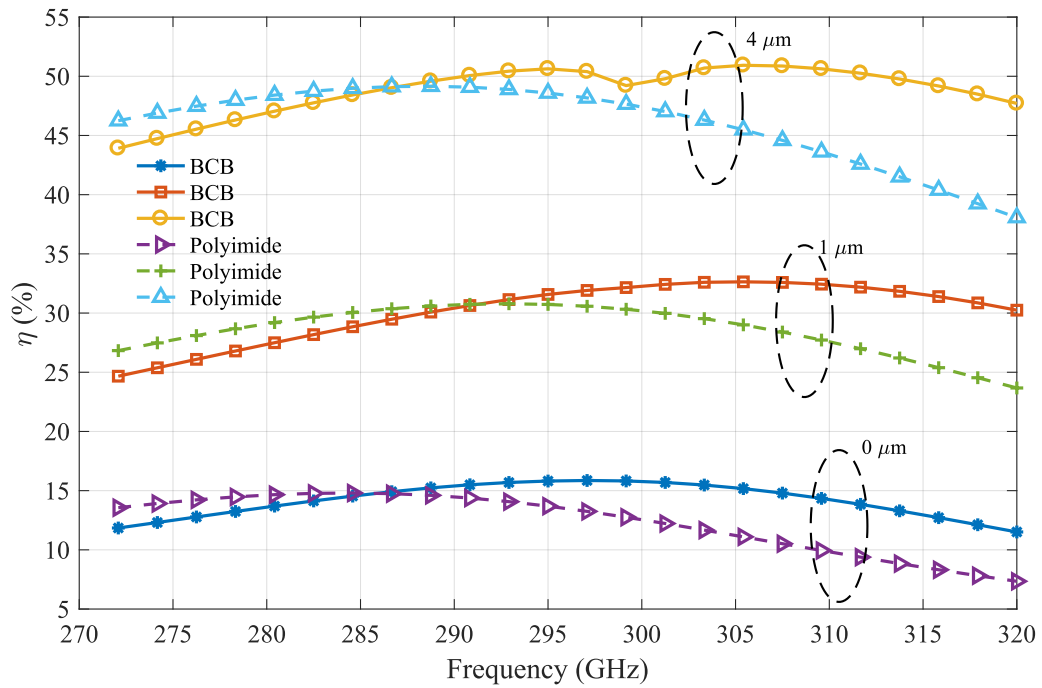


Figure 14: Radiation efficiency for both BCB and Polyimide considering different values of conductor thicknesses, $\{0, 1 \text{ and } 4\} \mu\text{m}$, respectively.



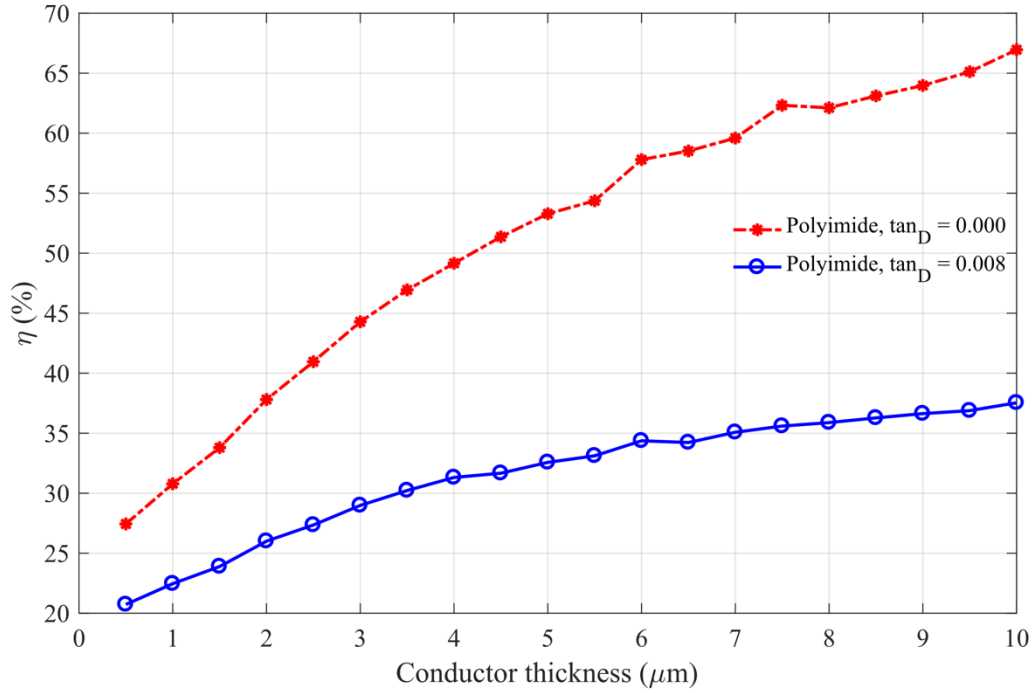


Figure 15: Peak radiation efficiency as a function of conductor thicknesses for both BCB and Polyimide considering zero tangent loss.

4.2 BCB and Polyimide Stack-up

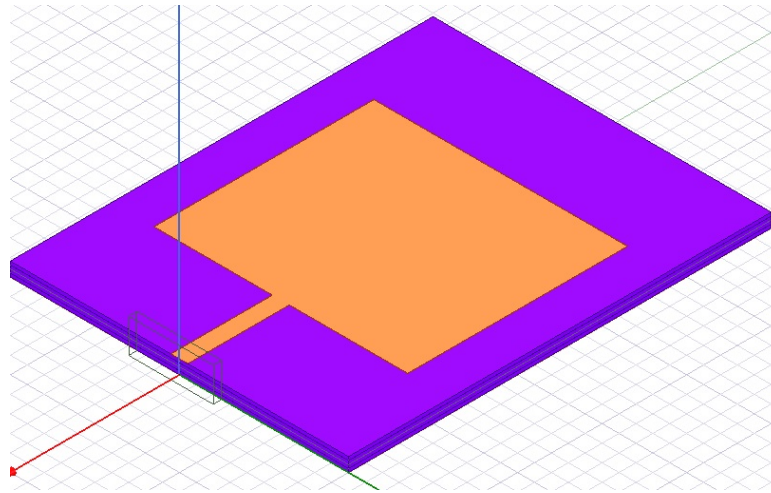
As we already mentioned in the above sections, a $< 4 \mu\text{m}$ substrate layer is required within the context of this project, since the usage of BCB/Polyimide impose a maximum substrate height that is possible to fabricate with homogeneity. This limitation comes from the fact the design flow consists of a spinning process which is then cured in an oven at a specific temperature range and time. However, we have concluded that the antenna efficiency is governed by the substrate thickness. Therefore, it is of the extreme importance to have an antenna design process that match with the practical constraints allowing to achieve a good radiation efficiency. This motivated us to propose a multilayer substrate design which allows improvements in the radiation efficiency while maintaining each layer with only $4 \mu\text{m}$ of thickness. Each layer could be manufactured independently and next stacked on top of each other. Simulations results of this architecture considering different number of layers are presented for both BCB and polyimide substrates. Both present satisfactory radiation efficiency that achieves peak of 70 % even considering tangent loss of 0.008.

Figure 16 illustrates an isometric view and a side view of the microstrip antenna used to demonstrate the concept. The 4 layers of BCB/Polyimide are stacked with a very thin layer ($0.1 \mu\text{m}$) of glass between them. As already mentioned, the use of glass is just for illustration purposes. Once again, we considered a simple microstrip antenna just for efficiency analysis. We intend to replace it with the slot configuration that we proposed for impedance bandwidth enhancement in case this solution is chosen to move forward.

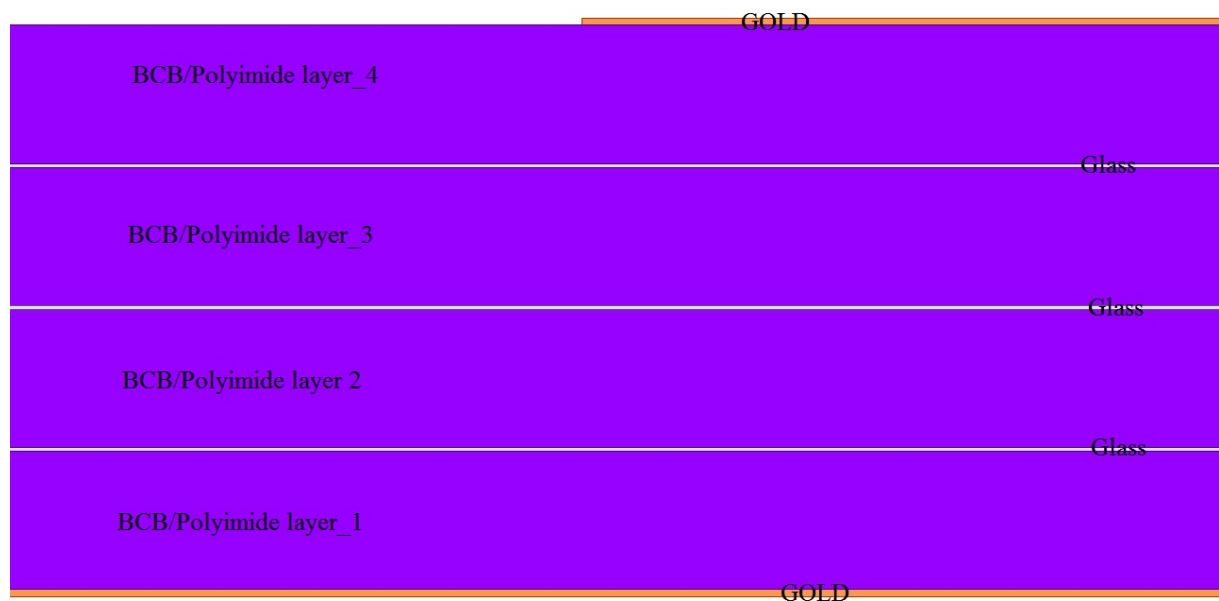
Figure 17 shows the radiation efficiency as a function of frequency considering {1, 2, 3 and 4} layers of BCB/Polyimide. As it is possible to conclude from the figure, each additional layer corresponds to almost 20 % efficiency improvement for both BCB and Polyimide. Considering 0 tangent loss and 4 layers of substrate, peak radiation efficiency of $\approx 90 \%$ is achieved, which means that the conductor loss is no more relevant.



Figure 18 shows the radiation efficiency considering 4 layers of Polyimide with 0.008 tangent loss. It is possible to observe that even considering the worst scenario ($\epsilon_r \approx 3.5$ and $\tan \delta = 0.008$), a peak radiation efficiency of 70% is possible, which represents a good result.



a) Isometric view



b) Side view

Figure 16: Isometric and side view of the proposed multilayer design. Each BCB/Polyimide layer has 4 μm thickness separated with 0.1 μm thick of glass substrate. The ground plane and the antenna are both composed by 0.2 μm thicknesses of gold metal.



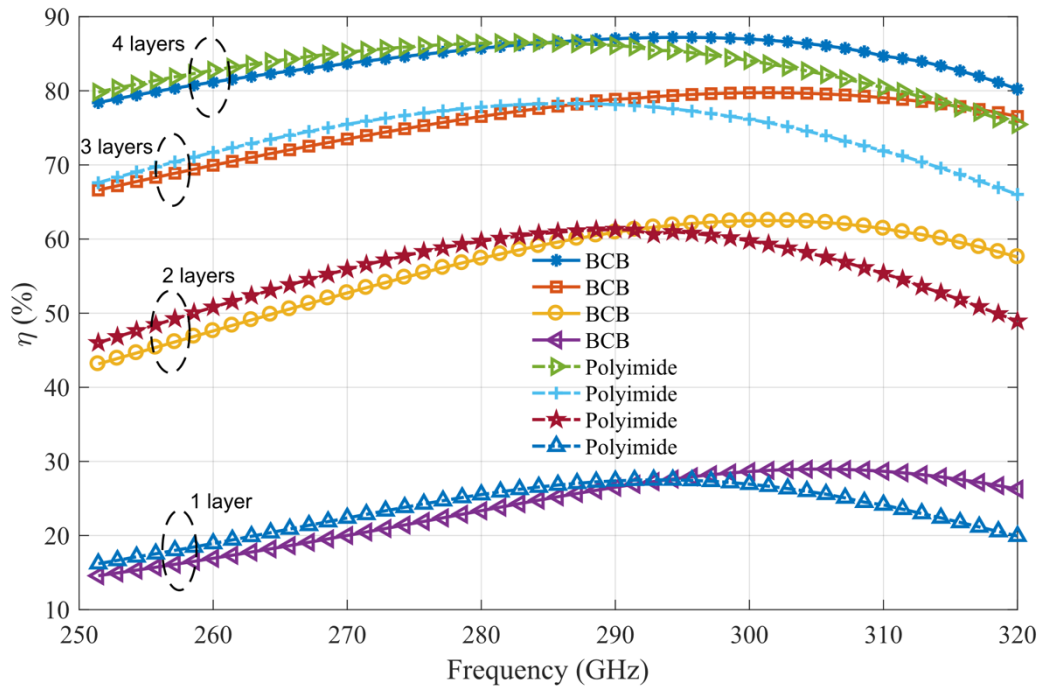


Figure 17: Radiation efficiency considering different layers of BCB/Polyimide without considering substrate loss.

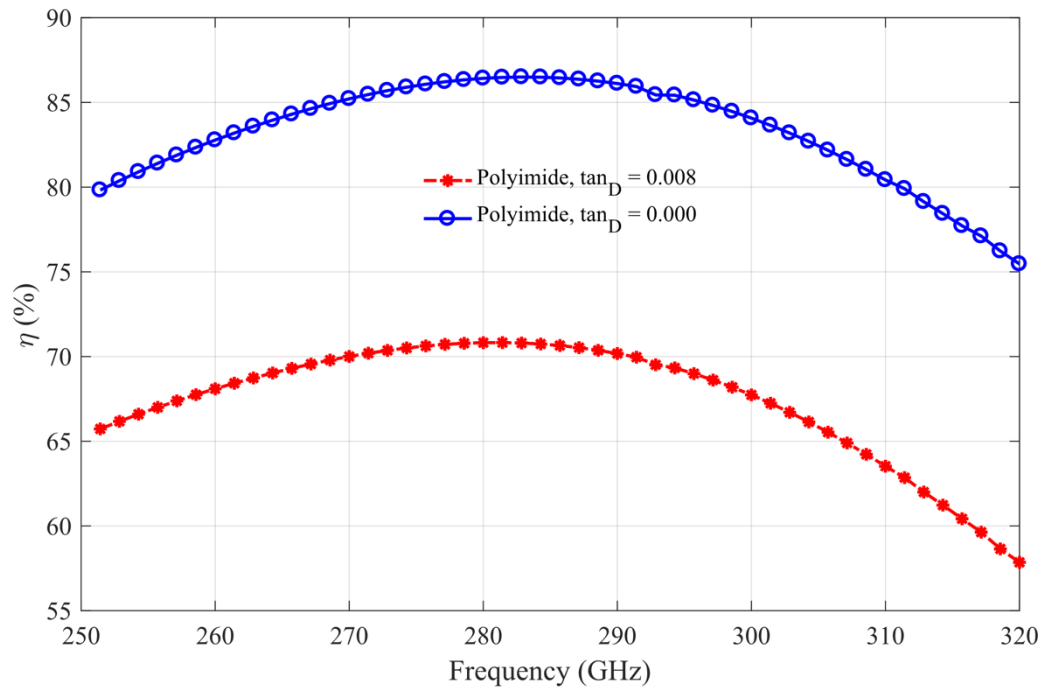


Figure 18: Radiation efficiency with and without considering substrate loss. The substrate loss causes almost 15 % reduction in efficiency.



5 Conclusion

The main goal of this report was to analyze the feasibility of designing sub-THz planar antennas using BCB and polyimide substrates, and how the substrate thickness can affect the antenna performance. In order to do that, we characterized the main figures of merit of a square patch antenna operating at 300 GHz through HFSS simulations such as radiation efficiency, bandwidth and directivity. We evaluated the parameters considering substrate thicknesses varying from 4-30 μm , and for different physical antenna widths. From these simulations, we concluded that the substrate thickness has a strong impact on the antenna efficiency and bandwidth. It was demonstrated that the efficiency has a linear dependency with the substrate thickness up to 14 μm . The achieved peak efficiency increases from 20% to 60% when the substrate thickness is increased from 4 μm to 14 μm , respectively, when considering ideal zero conductor thickness. Above 14 μm thickness the efficiency starts to grow slower achieving a maximum of 95% at 30 μm .

The main conclusions of this report can be summarized as follows:

- The antenna radiation efficiency is dominated by the conductor loss;
- The conductor loss decreases significantly as the substrate height increases;
- The antenna design is strongly governed by the substrate thickness;
- A trade-off between efficiency, bandwidth and substrate thickness must be established;
- Increases in the conductor thickness can be considered to decrease the substrate thickness without degradation in efficiency.

In summary, we found that 16 μm thickness of both BCB and Polyimide substrates are required to achieve an acceptable antenna efficiency (in the order of 70%). The width of the patch element will be adjusted looking for a bandwidth enhancement, but we do not expect to achieve an area of more than $600 \times 600 \mu\text{m}^2$. Also, it is important to note that the ground plane needs to be larger than the radiating element (patch) so, for example, if the radiating element takes $600 \times 600 \mu\text{m}^2$, the overall antenna dimension will occupy around $1000 \times 1000 \mu\text{m}^2$. However, these values are susceptible to being changed and the antennas redesigned until we achieve solutions that can be fabricated with the available technologies and acceptable performance. These tasks will be carried out in close collaboration with the different partners of the project, namely UGLA and UCL.



6 Ongoing and Future work

After discussion with UGLA, some directions forward have been agreed. It would be an interesting solution to achieve a 15 μm of BCB/polyimide antenna considering a more complex feeding method to overcome the difficulties associated with the design and fabrication of a 15 μm via length to feed the radiating element. We are currently designing and analysing the feasibility of a magnetic coupling version. UGLA also suggested that some metal pattern could be deposited between layers, which would represent a type of metamaterial structure to potentially improve the antenna performance. This possibly represents an innovation that would compensate the effort invested in developing this process and we are working toward that solution. UGLA also suggested that substrate integrated waveguide antennas are likely to be the best solution to be adopted in future and it is also under the INESC responsibility to investigate this approach.

Once we have achieved the final design step, which means that all the fabrication possibilities have been analysed and the antennas are redesigned or adjusted to match design fabrication processes, the antennas are going to be fabricated and integrated with the respective devices, RTD or UTC-PD, at UGLA and UCL partners, respectively.



References

- [1] K. Okada, S. Suzuki, and M. Asada, "Resonant-tunneling-diode terahertz oscillator integrated with slot-coupled patch antenna," *Conf. Proc. - Int. Conf. Indium Phosphide Relat. Mater.*, pp. 14–15, 2014.
- [2] K. Okada, K. Kasagi, N. Oshima, S. Suzuki, and M. Asada, "Resonant-Tunneling-Diode Terahertz Oscillator Using Patch Antenna Integrated on Slot Resonator for Power Radiation," *IEEE Trans. Terahertz Sci. Technol.*, vol. 5, no. 4, pp. 613–618, 2015.
- [3] Y. Koyama, R. Sekiguchi, and T. Ouchi, "Oscillations up to 1.40 THz from resonant-tunneling-diode-based oscillators with integrated patch antennas," *Appl. Phys. Express*, vol. 6, no. 6, 2013.
- [4] J. Grzyb, R. Al Hadi, and U. R. Pfeiffer, "Lens-integrated on-chip antennas for THz direct detectors in SiGe HBT technology," *IEEE Antennas Propag. Soc. AP-S Int. Symp.*, pp. 2265–2266, 2013.
- [5] M. Natrella *et al.*, "Modelling and measurement of the absolute level of power radiated by antenna integrated THz UTC photodiodes," *Opt. Express*, vol. 24, no. 11, p. 11793, 2016.
- [6] K. H. Alharbi, A. Ofiare, M. Kgwadi, A. Khalid, and E. Wasige, "Bow-tie antenna for terahertz resonant tunnelling diode based oscillators on high dielectric constant substrate," *2015 11th Conf. Ph.D. Res. Microelectron. Electron. PRIME 2015*, pp. 168–171, 2015.
- [7] M. Applications *et al.*, "Planar Wideband Circularly Polarized Cavity-backed Stacked Patch Antenna Array for," no. c, pp. 1–10, 2018.
- [8] X. Ding, Z. Zhao, Y. Yang, Z. Nie, and Q. H. Liu, "A Compact Unidirectional Ultra-wideband Circularly Polarized Antenna Based on Crossed Tapered Slot Radiation Elements," *IEEE Trans. Antennas Propag.*, vol. PP, no. c, pp. 1–1, 2018.
- [9] N. W. Liu, L. Zhu, W. W. Choi, and J. D. Zhang, "A low-profile differentially fed microstrip patch antenna with broad impedance bandwidth under triple-mode resonance," *IEEE Antennas Wirel. Propag. Lett.*, vol. 17, no. 8, pp. 1478–1482, 2018.
- [10] Z. Tang, X. Wu, J. Zhan, Z. Xi, and S. Hu, "A novel miniaturized antenna with multiple band-notched characteristics for UWB communication applications," *J. Electromagn. Waves Appl.*, vol. 32, no. 15, pp. 1961–1972, 2018.
- [11] "ittipiboon1990.pdf." .
- [12] C. Tsao, Y. Hwang, F. Kilburg, and F. Dietrich, "Aperture-coupled patch antennas with wide-bandwidth and dual-polarization capabilities," *Antennas Propag. Soc. Int. Symp. 1988. AP-S. Dig.*, pp. 936–939, 2002.
- [13] C. A. Balanis, "Antenna theory: a review," *Proc. IEEE*, vol. 80, no. 1, pp. 7–23, 1992.
- [14] D. M. Pozar, "Microstrip antennas," *Proc. IEEE*, vol. 80, no. 1, pp. 79–91, 1992.
- [15] I. A. and P. Society, *IEEE Standard for Definitions of Terms for Antennas*, vol. 2013. 2013.
- [16] B. Benakaprasad, A. Eblabla, X. Li, D. J. Wallis, I. Guiney, and K. Elgaid, "Design and performance comparison of various terahertz microstrip antennas on GaN-on-low resistivity silicon substrates for TMIC," *Asia-Pacific Microw. Conf. Proceedings, APMC*, pp. 4–7, 2017.
- [17] M. Konno, "Conductor loss in thin-film transmission lines," *Electron. Commun. Japan, Part II Electron. (English Transl. Denshi Tsushin Gakkai Ronbunshi)*, vol. 82, no. 10, pp. 83–91, 1999.



